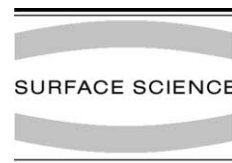




ELSEVIER

Surface Science 512 (2002) 201–220



www.elsevier.com/locate/susc

# Rare gases physisorbed on Pt(1 1 1): a low-temperature STM investigation

F. Brunet, R. Schaub, S. Fédrigo, R. Monot, J. Buttet, W. Harbich \*

*Département de Physique, Ecole Polytechnique Fédérale de Lausanne, 1015 Lausanne, Switzerland*

Received 13 July 2001; accepted for publication 2 March 2002

## Abstract

The structure and the phase transitions of Xe, Kr and Ar physisorbed on Pt(1 1 1) in the submonolayer-coverage range has been explored by low-temperature scanning tunneling microscopy. The hexagonal incommensurate rotated (HIR)  $\rightarrow$  hexagonal incommensurate (HI) transition with decreasing Xe coverage has been observed unambiguously. The onset of adlayer rotation occurs for Xe islands larger than  $700 \text{ \AA}^2$ . Xe dimers physisorbed on Pt(1 1 1) are commensurately ordered on the Pt(1 1 1) surface. The experimental results are compared to molecular dynamic simulations.

The orientation of the high order of commensurability (HOC) Kr structure with respect to the surface strongly depends on the terrace width and on the step morphology. Kr monolayer misorientation ranging from  $0^\circ$  to  $30^\circ$  has been observed depending on the surface morphology.

The Ar monolayer adopts a HOC structure aligned with respect to the Pt(1 1 1) surface while for low coverage, the most energetically favorable position of the Ar islands corresponds to a  $R(1.875 \times n)^\circ$  ( $n$  an integer) HI structure. © 2002 Published by Elsevier Science B.V.

*Keywords:* Physical adsorption; Noble gases; Platinum; Surface structure, morphology, roughness, and topography; Scanning tunneling microscopy

## 1. Introduction

Rare gases on various surfaces have been regarded as two-dimensional (2D) model systems in surface science due to their closed-shell electronic structure and weak interaction with substrates and among themselves (van der Waals interaction). These systems provide ideal testing grounds for 2D adsorbate phases and phase transitions as well as for growth mechanism of physisorbed films. The growth behavior of rare gases on a substrate can be scaled according to the interaction strength

which is defined as the ratio of the isosteric heat of adsorption  $u_1$  of the gas molecules onto the substrate surface at low coverages to the cohesive energy  $h_0$  of the bulk phase of the gases [1]. Complete wetting (or “type-1” growth) takes place only when the ratio  $u_1/h_0$  is close to 1. The isosteric heat of adsorption at low coverage of Ar [2], Kr [2] and Xe [3–5] on the Pt(1 1 1) surface is about 79, 128 and 277 meV, respectively, suggesting a type-1 growth for Ar and Kr. Xe should a priori not exhibit a complete wetting behavior ( $u_1/h_0 \sim 1.7$ ). Nevertheless, it was suggested (see discussion below) that complete wetting occurs only when “the net stress tending to strain the film parallel to the substrate vanishes”. The rotation of

\* Corresponding author.

the Xe monolayer with respect to the symmetry directions of the substrate which has been predicted by Novaco and McTague to be caused by the tendency to minimize the strain energy, allows a type-1 growth process of this system. Studies performed by elastic and inelastic thermal-He scattering on the wetting behavior of rare gas physisorbed films on the Pt(111) surface have demonstrated that Ar, Kr and Xe exhibit a “complete wetting” growth. During this growth process, the rare gas atoms are adsorbed on the surface and nucleate into 2D islands covering more and more the surface. After completion of the first adlayer, the film growth is layer by layer.

The structure of the rare gas adlayer is governed in a simplified description by the competition of two main interactions: the lateral adatom–adatom interaction  $h$  and the lateral variation of the substrate–adatom potential (corrugation)  $u_c$ . Depending on their respective magnitude, the adsorbed adlayer structure can be commensurate or incommensurate. Indeed, on one hand, the lateral interaction between adsorbed rare gas adatoms will tend to establish an adlayer structure with natural interatomic distances, i.e. incommensurate with the substrate and on the other hand, the surface corrugation potential will tend to force the adatom to occupy energetically favored adsorption sites leading to a commensurate structure. In special cases, where the lateral adatom–adatom interaction and the lateral variation of the substrate–adatom potential have similar magnitudes ( $h/u_c \simeq 1$ ), the adlayer structure will depend on the substrate’s crystallographic symmetry and on the adlayer and substrate interatomic distances (misfit). By varying the surface temperature  $T_s$  and the coverage  $\theta$ , a complex structural phase transition from commensurate to incommensurate structure can be observed. Owing to the magnitude of the lateral adatom–adatom interaction and the substrate–adatom potential for Ar ( $h = 17$  meV) [6], Kr ( $h = 26$  meV and  $u_c = 10$ – $20$  meV) and Xe ( $h = 43$  meV and  $u_c = 30$  meV) [2], the rare gas monolayers on the Pt(111) surface represent an interesting system to study the whole spectrum of phenomena and phase transitions of 2D matter with competing interactions.

In the past, physisorbed rare gases on various substrates (graphite [7–11], Pt(111) [3,6,12–16]) have been extensively studied. While Grimm et al. [7] use low-temperature scanning tunneling microscopy (STM) as in this study the others are based on diffraction methods (helium atoms and electrons). The commensurate–incommensurate phase transition has been theoretically explained in terms of domain-wall formation. For small misfit (less than  $\simeq 3\%$ ) the phase exhibits a domain structure of commensurate domains separated by incommensurate domain-wall regions, which may either exhibit linear (stripes) or hexagonal (honeycomb-like) arrays, depending on the interaction between the domain walls. These theoretical predictions have been verified experimentally for a variety of different systems such as Xe on Pt(111) [17] and graphite [7] surfaces. Nevertheless, the information obtained for Pt(111) by diffraction methods (low-energy electron diffraction, transmission high-energy electron diffraction or helium atom diffraction) is averaged over a macroscopic region of the surface and no direct real-space information is available which is needed for better understanding the physics of the rare gas adsorption. Moreover, the low-coverage features are inaccessible to a structural study by He diffraction [18].

STM and its application to low-temperature surface science systems opens the possibility of real-space studies down to the atomic scale. It is possible to obtain real-space images of the rare gas adlayer structure from submonolayer to monolayer coverages. A few STM studies have been performed on the Xe/Pt(111) [18–23], graphite [7], Cu(110) [24] and Cu(111) [25] systems but, none of these, have been reported in the literature on the Kr and Ar/Pt(111) system. The results presented in this paper focus on low-temperature STM studies of the structure of Xe, Kr and Ar adsorbed adlayers on Pt(111), varying the coverage from submonolayer to monolayer.

## 2. Experimental

The experimental set-up has already been described in detail elsewhere [26]. Originally designed

to investigate the processes which occur during the deposition of mass selected clusters [27], we have used this experimental set-up to study the rare gas adlayer structures. Only the elements essential for this paper are briefly described: sample preparation and STM measurements are performed in two different vacuum chambers connected by a transition chamber. A custom built manipulator holds the Pt(1 1 1)-sample during preparation and for thermal energy helium scattering (TEAS)-measurements and allows for transferring the sample into the STM chamber at cryogenic temperatures (25 K). The sample temperature can be varied between 25 and 1200 K by appropriate cooling and electron beam heating. The sample is cleaned by repeated cycles of Ar<sup>+</sup>-ion beam sputtering and O<sub>2</sub> chemical etching. After cleaning the sample is annealed for 1 mn at 1000 K and cooled to the lowest available temperature (25 K) in 40 mn. The state of the surface is controlled by recording the reflectivity of the surface for the helium beam. Rare gas is introduced into the vacuum chamber (partial pressure of  $1 \times 10^{-7}$  mbar) and the total coverage is monitored by the reflectivity of the helium beam. The completion of the first monolayer is achieved when the helium signal has almost fallen to its lowest value [13]. Whatever the rare gas (Ar, Kr and Xe), a film of 5 monolayers is deposited onto the Pt(1 1 1) surface.

The sample is transferred at 25 K into the STM. The surface temperature in the STM can be varied between 8 and 450 K by laser heating until the desired maximum temperature is reached. The laser is then stopped and the sample is cooled back down to 8 K. All STM images in this paper were recorded at 8 K.

It should be emphasized here that the sample preparation differs from the usual one in the sense that submonolayer coverages are obtained by evaporation instead of growth which might result in changes in the kinetics of the process.

STM images are generally straightforward to interpret, even though the contrast is a combination of topography and electronic effects which can be sometimes difficult to separate. In the case of rare gas physisorbed on a metallic Pt(1 1 1) surface, it is reasonable to suggest a smooth electronic density over the surface and grant the change in

height as real. Consequently, the dominant contribution to the tunneling current is geometric and originates from the different adsorption sites: the height difference between rare gas atoms can be directly related to their relative position over the outermost layer of the Pt(1 1 1) surface.

### 3. Results and discussion

#### 3.1. Xe on Pt(111)

In the following subsection, we present low-temperature STM images performed at different coverages ( $\theta_{\text{Xe}} = 0.41$  (1 ML), 0.20 and 0.08) in order to determine the evolution of the Xe adlayer structure with respect to the domain size. These results are compared to and intended to complete a schematic phase diagram resulting from diffraction data by Kern et al. [4]. A subsection concerning isolated adatoms and dimers is also developed. Finally, the experimental results are compared with molecular dynamic simulations.

##### 3.1.1. Xe monolayer ( $\theta_{\text{Xe}} = 0.41$ )

Earlier TEAS measurements (see for example [28]) have shown that a Xe monolayer adsorbed on a Pt(1 1 1) surface adopt a hexagonal incommensurate structure ( $d_{\text{Xe-Xe}} = 4.33(3)$  Å) rotated by  $\pm 3.3^\circ$  with respect to the commensurate phase orientation. A superstructure has been detected with a period of 23(2) Å (measured along a Xe row) and has been assigned to a buckling of the Xe layer.

Fig. 1(a) presents an atomically resolved image of a full monolayer of Xe on Pt(1 1 1) taken at 8 K. The Xe atoms form a hexagonal structure with a Xe–Xe interatomic distance of 4.37(5) Å. Moreover, Xe atoms form patches of about 15 atoms which appear in the STM topograph brighter than the surrounding Xe atoms. This leads to the formation of a hexagonal superstructure with a period of 26(2) Å (Fig. 1(b)), slightly larger than the one deduced from TEAS measurements [28]. The buckling is induced by the misorientation of the Xe monolayer with respect to the substrate. From Fig. 1(a) it is impossible to quantify this misorientation. We can a priori not confirm that the xenon

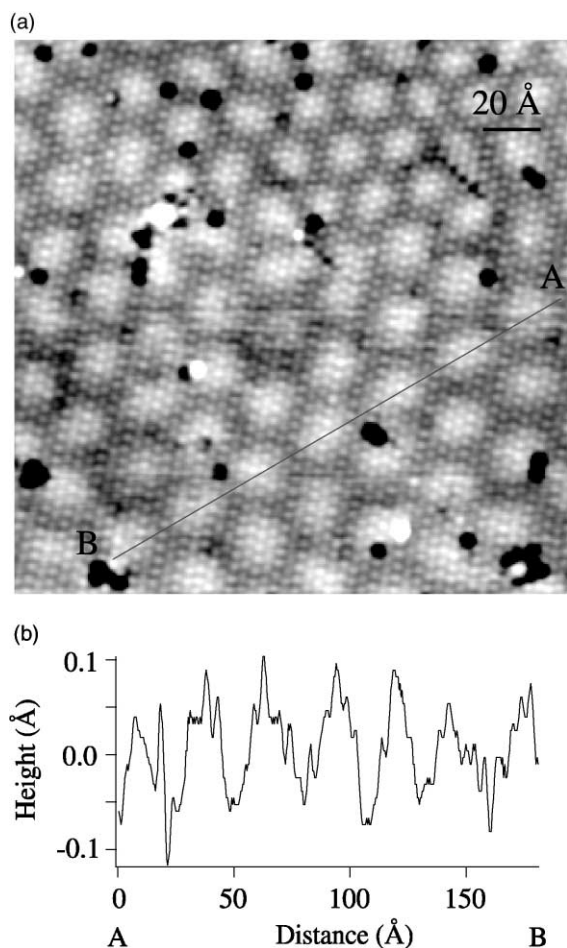


Fig. 1. (a) STM image ( $V_T = -0.602$  V,  $I_T = 0.33$  nA) of a monolayer of xenon on a Pt(111) surface taken at 8 K. The buckling of the monolayer is clearly observed, leading to a hexagonal superstructure. (b) Line scan along one direction of the superstructure. The period is  $26(2)$  Å.

adlayer is rotated by  $30 \pm 3.3^\circ$  with respect to the substrate as observed by TEAS measurements. It has been shown [28] that this specific orientation corresponds to the locking of the adsorbed layer by a certain fraction of adsorbed atoms sitting in high-symmetry sites: the incommensurate rotated monolayer is in fact a monolayer with a high order of commensurability (HOC).

For a better illustration, two schematic models are shown in Fig. 2(a) and (b). Fig. 2(a) shows a chain of 15 xenon atoms rotated by  $30 + 3.3^\circ$  with

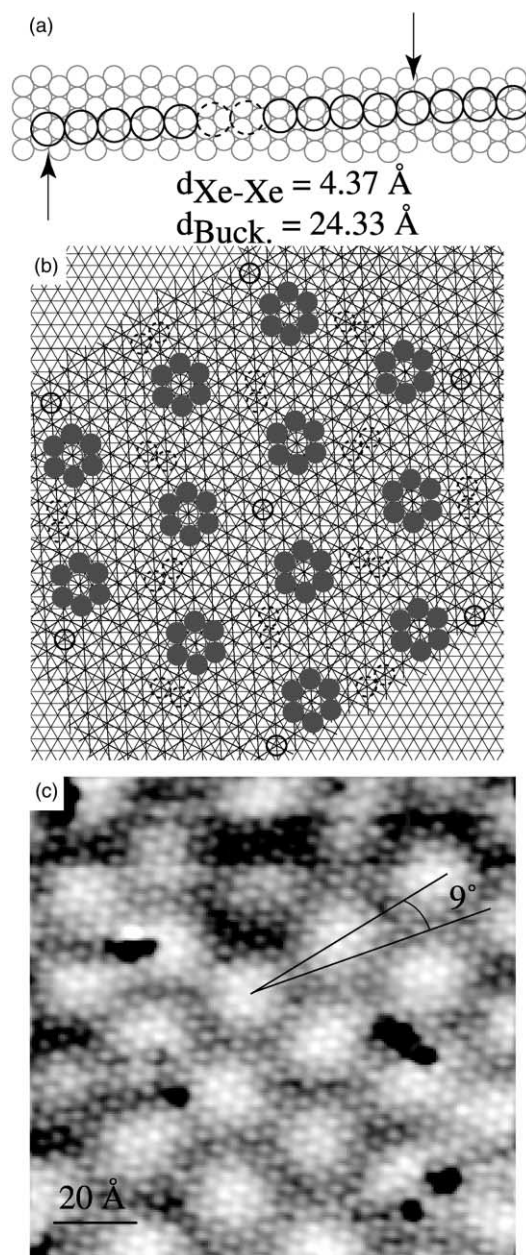


Fig. 2. (a, b) Model of the HOC rotated phase of a chain of Xe atoms (from Ref. [28]) and monolayer adsorbed on a Pt(111) surface, respectively. The lattice parameter is  $4.37$  Å. In (a), the atoms marked by an arrow are in high-order symmetry (fcc or hcp). The dotted circles represent the fifth and the sixth atom (see text). In (b), the grey atoms surround atoms in on-top-sites which are located higher than the others, especially the ones in hollow sites (black atoms). (c) Misorientation between the HOC structure and the superstructure ( $V_T = -0.602$  V,  $I_T = 0.33$  nA).

respect to the substrate. The lattice parameter is 4.37 Å as in the experiment. From this model, one clearly notices that some atoms sit in hollow sites (marked by an arrow) and are separated by a distance of  $11 \times 4.37 = 48.08$  Å. It has been expected that the experimental buckling period (23(2) Å) deduced from TEAS along a Xe row is compatible with this model if one notices that the fifth and the sixth Xe atoms are located nearly as deep as the two atoms which are in hollow sites, leading to a period of  $48.08/2 = 24.04$  Å. If we extend such a representation in two dimensions (Fig. 2(b)) one observes that few xenon atoms sit on top-sites and form a hexagonal superstructure. Those atoms are located somewhat higher than the other atoms, leading to the buckling of the monolayer. In this configuration the superstructure is exactly aligned with respect to the monolayer structure. The buckling period proposed in [28] cannot be compared with our experimental value because they are not a feature of the same superstructure. Kern et al. [28] have measured a period along a Xe row whereas our experimental period has been measured along successive maxima of the buckling. As shown in Fig. 2(c), the superstructure is misoriented with respect to the Xe monolayer structure by an angle of  $9(1)^\circ$ . This misorientation suggests that the angle between the Pt(1 1 1) surface and the domain observed in Fig. 1 is not  $33.3^\circ$  (or  $26.7^\circ$ ) but slightly different. This will be confirmed further below in the molecular dynamic simulations sections.

### 3.1.2. $\theta_{\text{Xe}} = 0.2$

The STM image reported in Fig. 3(a) has been recorded after annealing the sample at 125 K. This temperature is high enough to evaporate the monolayer from the Pt(1 1 1) surface. Nevertheless, the surface exhibits several xenon domains bonded together by bridges composed of few atoms. The corresponding coverage of the surface is  $\theta_{\text{Xe}} = 0.2$ . These domains present regular shapes with sharp edges and are  $2.1(1)$  Å high. The structure adopted by the xenon adatoms is an incommensurate hexagonal structure with a lattice parameter of  $4.43(5)$  Å. The most interesting feature revealed in this image is that domains do not have the same orientation with respect to the substrate. Owing to

the atomic resolution of these domains, one can easily observe in Fig. 3(a) that only two types of orientation are present as indicated by the dotted and full arrows. Resolution of the bare platinum surface has been achieved in the vicinity of the image by changing the gap voltage and the tunneling current. The  $[1\bar{1}0]$  direction of the platinum surface is reported in both Fig. 3(b) and (c) which are magnifications of the central and the bottom-right part of Fig. 3(a), respectively. The orientation of the two domains with respect to the Pt(1 1 1) surface is  $33^\circ$  and  $27^\circ$ . This misorientation leads to a buckling of the xenon domains as shown in Fig. 3(d). The structure adopted by the Xe adlayer for such coverage is a hexagonal incommensurate rotated (HIR) structure. The mean size of the domain whatever their orientation is about  $1200 \text{ \AA}^2$  corresponding to  $\sim 70$  Xe atoms.

### 3.1.3. $\theta_{\text{Xe}} = 0.08$

In Fig. 4(a) we present an STM image recorded in the same region as before. Nevertheless the configuration of the surface is different, composed of isolated close-packed xenon islands adsorbed on terraces. The corresponding coverage is  $\theta_{\text{Xe}} = 0.08$ . The mean size of the islands is  $500 \text{ \AA}^2$  corresponding to  $\sim 30$  Xe atoms. The islands are imaged  $2.3(1)$  Å high. The Xe islands adopt a hexagonal incommensurate (HI) structure and the lattice parameter, determined on different islands, is  $4.45(2)$  Å. An interesting feature is that all the islands have the same orientation with respect to the substrate, i.e. rotated by  $30^\circ$ . We have reported in Fig. 4(b) three xenon islands located at different positions on the surface showing this rotation. This particular orientation has been observed on every xenon island present on the surface.

### 3.1.4. Isolated adatoms and dimers

We have performed an annealing at 135 K in order to evaporate the rare gas from the terraces. Fig. 5(a) shows this situation. Only higher coordinated Xe atoms at steps (not visible in this STM image) and adsorbates on the surface are present. We also observe few isolated adatoms (A and B in Fig. 5(a)) and Xe dimers (C and D in Fig. 5(a)). The decoration of the silver cluster by rare gas atoms is discussed in a different communication [29]. The

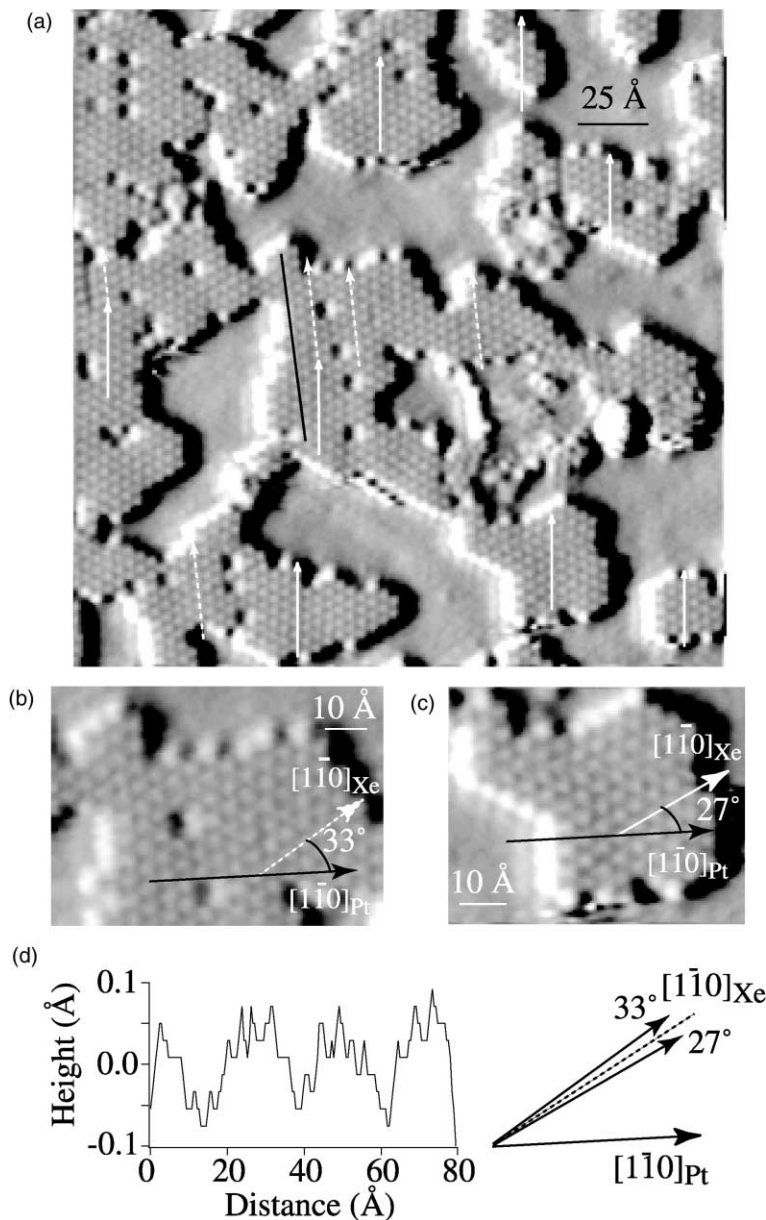


Fig. 3. (a) STM image in derivative mode after annealing to 125 K ( $V_T = -0.299$  V,  $I_T = 0.51$  nA). The dotted and full arrows correspond to different domain orientations. (b, c) Magnification of the central and right-bottom part of (a). The  $[1\bar{1}0]_{\text{Pt}}$  direction of the substrate is shown. (d) Line scan along the dark line marked on (a) obtained from the real image.

two Xe dimers observed in this image are misoriented by an angle of  $60^\circ$  and are aligned along the  $[1\bar{1}0]_{\text{Pt}}$  direction of the substrate. By measuring the separation of the peaks in Fig. 5(b), we find that the Xe atom separation is  $d_{\text{Xe-Xe}} = 5.6(2)$  Å. This is,

within the error of the measurement, twice the Pt interatomic separation ( $2d_{\text{Pt-Pt}} = 5.55$  Å) measured along the  $[1\bar{1}0]_{\text{Pt}}$  direction. The height of the Xe atoms in the dimers is  $2.4(1)$  Å which is similar to the height of the Xe islands observed for several

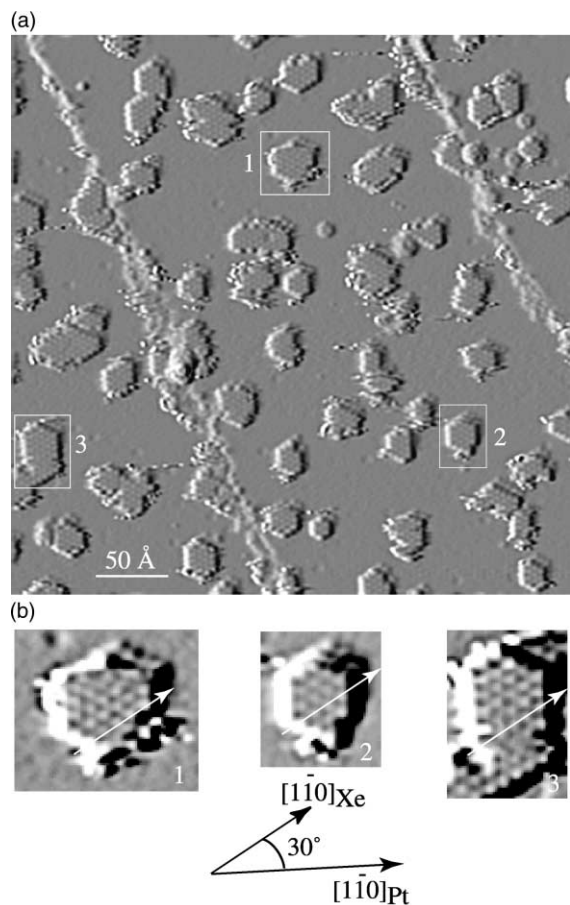


Fig. 4. (a) STM image in derivative mode ( $V_T = -0.224$  V,  $I_T = 0.44$  nA) of a Pt(111) surface covered by Xe islands ( $\theta_{Xe} = 0.08$ ). (b) Magnification of three Xe domains present in (a). The Pt(111) orientation is also reported.

coverages ( $\theta_{Xe} = 0.2$  and  $0.08$ ). However, the height of an isolated atom is substantially lower ( $1.50(5)$  Å as seen in Fig. 5(b)).

### 3.1.5. Discussion

This study has revealed that the Xe adlayer structure on Pt(111) is strongly dependent on the coverage of the surface, in agreement with previous TEAS studies (see for example [14]). High-resolution He diffraction studies have reported that variation of experimental parameters such as the surface temperature and the coverage leads to various phase transitions. It has been shown that the commensurate  $(\sqrt{3} \times \sqrt{3})R30^\circ$  structure (C) is

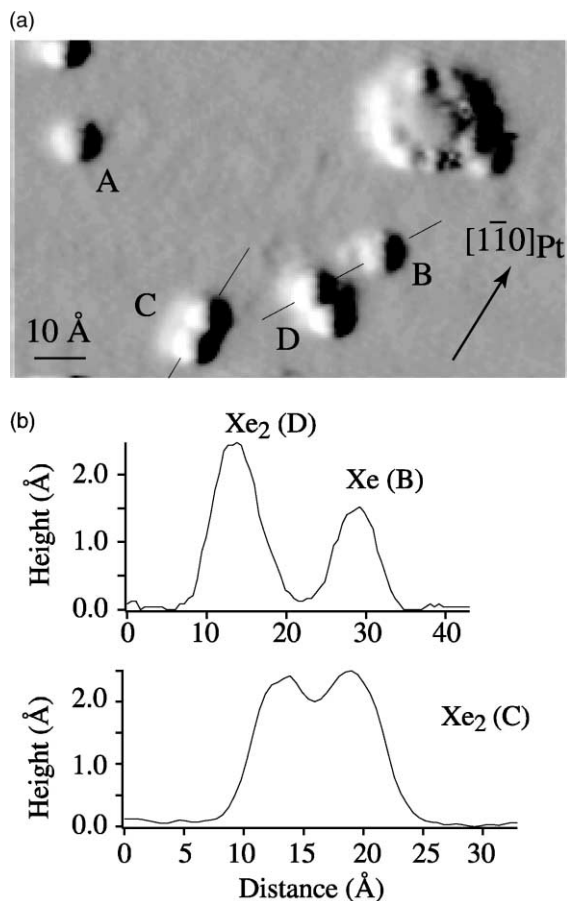


Fig. 5. (a) STM image in derivative mode ( $V_T = -0.205$  V,  $I_T = 0.16$  nA) of a Pt(111) surface covered by isolated Xe adatoms (A and B) and Xe dimers (C and D). The Pt orientation is also reported. A  $Ag_{19}$  cluster [29] is also present on the surface and is decorated by Xe atoms. (b) Line scans across the Xe dimer marked (C) and across an isolated Xe atom (B) compared with one Xe atom of the dimer (D).

stable over an extended range of coverage ( $0 < \theta_{Xe} < 0.33$  where  $\theta_{Xe} = 1$  correspond to  $1.5 \times 10^{15}$  Xe atoms/cm<sup>2</sup>) and temperature ( $62 < T_s < 99$  K) range. The lattice constant and average domain size in this phase are  $d_{Xe-Xe} = 4.80$  Å and  $\sim 800$  Å, respectively. At completion of the (C) phase, a continuous phase transition to a stripe incommensurate phase (SI) occurs. A similar phase transition is observed by cooling the Pt(111) surface below 62 K down to 25 K, the lowest temperature accessible in the experiment reported in [17]. The

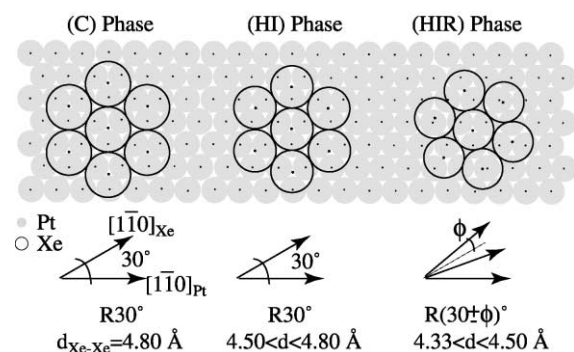


Fig. 6. Schematic representation of the (C), (HI) and (HIR)-phase of the Xe adlayer (the rotation in the (HIR)-phase is underline for better illustration).

stripe phase (SI) is stable in the misfit  $m$  range  $0 < m \leq 6.5\%$  (corresponding to a Xe–Xe distance range  $4.8 < d_{\text{Xe-Xe}} \leq 4.50 \text{ \AA}$ ). The estimated average domain sizes of the incommensurate layer is  $\sim 350 \text{ \AA}$  parallel to the wall and  $\sim 50 \text{ \AA}$  perpendicular. With increasing coverage, the stripe phase (SI) transforms at a critical misfit of  $\simeq 6.5\%$  to a hexagonal incommensurate  $R30^\circ$  phase (HI) in a first-order transition. Upon further increase of the misfit ( $m \geq 7.2\%$ ) corresponding to  $\theta_{\text{Xe}} = 0.38$ , the HI phase displays a continuous transition from an aligned ( $R30^\circ$ ) to a rotated orientation (HIR). Fig. 6 gives a cartoon-like model of the different Xe structures on Pt(111) depending on its lattice parameter, i.e. the coverage. The observed rotation of the adlayer has already been theoretically predicted by Novaco and McTague [30]. They have shown that the energy of a monolayer is dependent on its orientation relative to the substrate. In particular, the orientation which minimizes the strain energy is expected to deviate from the main symmetry directions of the substrate.<sup>1</sup> The devi-

<sup>1</sup> Owing to magnitude of its isosteric heat and 0-K cohesive energy of the bulk phase, Xe should a priori not exhibit a complete wetting behavior ( $u_1/h_0 \sim 1.7$ ). Nevertheless, several authors [31] suggested that complete wetting occurs only when “the net stress tending to strain the film parallel to the substrate vanishes”. The rotation of the Xe monolayer with respect to the symmetry directions of the substrate which has been predicted by Novaco and McTague to be caused by the tendency to minimize the strain energy, allows a type-1 growth process of this system as observed experimentally [16].

ation increases with the coverage and reaches a maximum at monolayer completion ( $R(30 \pm 3.3)^\circ$ ) which corresponds to a coverage of  $\theta_{\text{Xe}} = 0.41$  and to a lattice parameter of  $d_{\text{Xe-Xe}} = 4.33(3) \text{ \AA}$ .

In our case, the sequence of HIR  $\rightarrow$  HI transition with decreasing the rare gas coverage ( $d_{\text{Xe-Xe}} = 4.43(5) \rightarrow 4.45(5) \text{ \AA}$ ) has been observed unambiguously. The transition from the HI  $R30^\circ$  orientation to the rotated orientation (HIR) can be related to the size of the islands. The largest HI Xe island we observed which was not rotated has been found to be  $700 \text{ \AA}^2$  corresponding to about 40 Xe atoms. We used this value as a yardstick for the onset of rotation. This implies that the HI  $\rightarrow$  HIR transition occurs when the coverage is comprised between  $\theta_{\text{Xe}} = 0.08$  and  $0.2$ , which is at least two times smaller than the limit coverage measured by Kern et al. [17] ( $\theta_{\text{Xe}} = 0.38$ ) for this phase transition. The difference between our work and the work by Kern might be found in the sample preparation technique as discussed above. In this case one would assume the rotation of the adlayer to be metastable with a hysteresis in  $\theta$ . The value deduced from TEAS measurements has been obtained with a surface temperature of  $25 \text{ K}$ , the lowest temperature reported by the author. This is substantially higher than the surface temperature ( $8 \text{ K}$ ) at which we have performed our STM measurements. For such a temperature and coverage, we have shown that the structure adopted by the Xe islands is a HI  $R30^\circ$  structure with a lattice parameter which is only 2% smaller than the one adopted by the full monolayer, in agreement with a previous study [18]. For a similar coverage ( $\theta_{\text{Xe}} = 0.03$ ), Weiss and Eigler [18] have observed by STM measurements recorded at  $4 \text{ K}$  that all of the Xe islands (the largest observed Xe island was composed of 13 atoms) adsorbed on a Pt(111) surface were rotated by  $30^\circ$  with respect to the substrate orientation and adopt a HI structure. Consequently, for very low temperature the structure of the Xe adlayer is essentially dependent on the lateral Xe–Xe interaction and not on the substrate–adatom potential. Increasing the coverage, i.e. the size of the islands, the rare gas adatoms tend to establish an adlayer structure with the natural interatomic distance. When the size of the islands is of about  $1000 \text{ \AA}^2$ , the adlayer rotates in order to

minimize its strain energy leading, at completion of the first monolayer, to the HOC structure.

For very low coverage, we have observed that Xe dimers are aligned along the  $[1\bar{0}]_{\text{Pt}}$  direction of the substrate with an interatomic distance which is approximately twice the interatomic Pt distance. This is substantially larger than the 4.33 and 4.36 Å [32] Xe–Xe spacing in the solid phase and in the molecule Xe<sub>2</sub>, respectively. According to their orientation and the adatom–adatom separation, we deduce that the Xe dimers are commensurately ordered on the Pt(1 1 1) surface. The atomic position normal to the surface of the Xe atoms is unfortunately not available from our measurements. The superposition of a Pt(1 1 1) lattice in Fig. 5(a) does not allow us to conclude on a specific position of the monomer and the dimer on the surface. Whatever the situation (we arbitrarily place the monomer A in the three different sites (on top, fcc and hcp-hollow sites) and notice the corresponding position of the monomer B and the two dimers (C and D)) they never sit on the same positions. Consequently, we cannot provide further experimental evidence for the ab initio calculations done by Müller [33] on the interaction of the Pt(1 1 1) surface with adsorbed Xe atoms. He found that the binding energy between Xe adatom and substrate is strongest at the on top adsorption site. He has obtained similar results on coadsorbed Xe atoms. Nevertheless the calculation were done with two Xe atoms located in on top sites but separated by 4.8 Å and aligned along the  $[1\bar{1}2]_{\text{Pt}}$  direction which is not in agreement with our experimental observations since the Xe dimers are commensurately ordered along the  $[1\bar{1}0]_{\text{Pt}}$  direction of the Pt(1 1 1) surface. However, Müller [33] mentions that the coadsorption induces an increase in the Xe adsorption distance above the surface. This is consistent with our measurements since the Xe dimers are  $\sim 1$  Å higher than the isolated Xe atom (2.4(1) and 1.50(5) Å, respectively). We have also shown that the height of the dimers and islands (whatever the size) are similar. Similar results have been obtained by Weiss and Eigler [18]. The authors have shown that an island of 13 atoms is imaged 2.4 Å high compared to 1.9 Å for isolated Xe atoms (the images were recorded with a bias voltage of  $-0.005$  and  $-0.010$  V, respectively).

### 3.1.6. Molecular dynamic simulations

Our experimental results supply an interesting reference for structural simulations. In particular, the possibility of real-space observation of the structure adopted by Xe atoms on a Pt(1 1 1) is a great opportunity to check the relevance of the potential used for this system in molecular dynamic simulations.

We present in the following results of molecular dynamic simulations obtained on the structure of Xe clusters on a Pt(1 1 1) surface. The Xe/Pt forces were derived from an empirical potential developed by Barker and Rettner [34,35] which is consistent with a wide range of dynamical and equilibrium experimental data. The Xe/Xe energy includes the Barker pair potential and the Axilrod–Teller–Muto three body interaction both modelling pure Xe systems, and the surface mediated energy composed by the McLachlan modification of the dispersion potential and the interaction of the adsorption-induced and image dipoles called here dipole–dipole energy. The calculation of the dipole–dipole forces assumed that the dipoles are perpendicular to the Pt surface. The platinum slab was kept frozen while an artificial thermal bath was created for the Xe clusters by using Langevin forces. A Verlet type algorithm was used to integrate the equation of motion. The cluster initial configuration was prepared by keeping a circular shaped group of atoms from a (1 1 1) Xe layer at a distance  $z_0 = 3.4$  Å above the Pt surface, the Xe–Xe distance  $d$  and the angle  $\phi$  between the orientation of the Pt surface and the Xe layer being adjustable. The typical rate used for cluster temperature variation was 0.3 K/ps. The Xe atom positions shown were averaged during 18 ps at constant temperature. Dipole–dipole interaction had to be abandoned for cluster sizes above 500 atoms due to calculation time [36].<sup>2</sup>

The structure of a cluster composed of 1800 Xe atoms physisorbed on a Pt(1 1 1) surface has been

<sup>2</sup> The dipolar moment calculation of  $N$  interacting polarizable dipoles needs to solve a system of  $N$  linear equations with  $N$  unknown dipolar moments. This calculation should be done at each molecular dynamic time step. An infinite hexagonal array of polarizable dipoles above a perfect metal surface has been studied in details [36].

simulated and compared to our experimental results obtained for the Xe monolayer (Figs. 1 and 2). The result of the simulation is reported in Fig. 7. The initial Xe–Xe distance and the angle  $\phi$  are 4.37 Å and 33.3°, respectively and the surface tem-

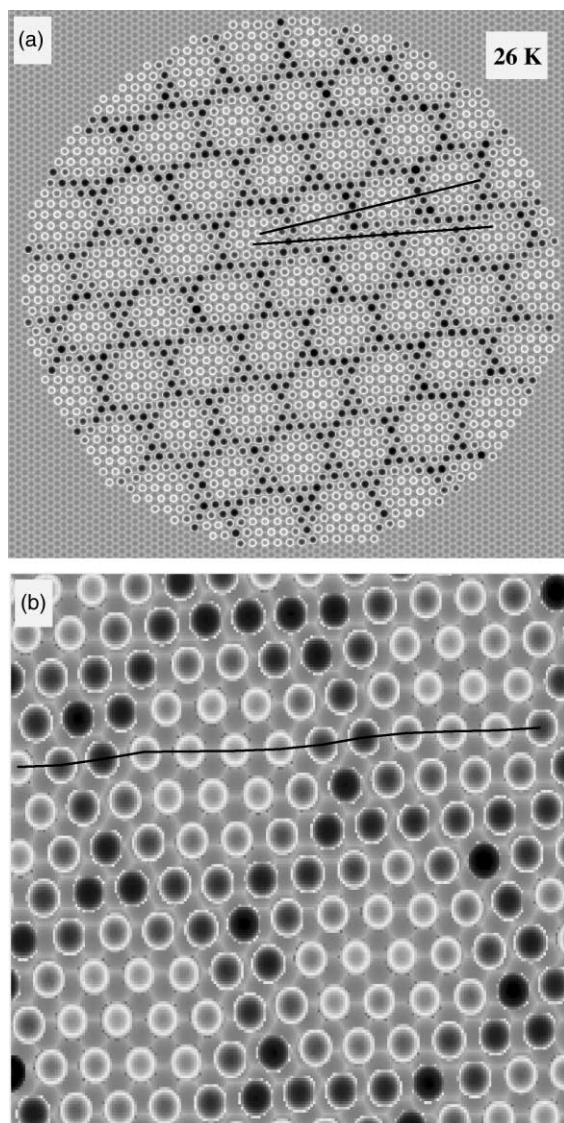


Fig. 7. (a) Structure of a Xe cluster on a Pt(111) surface obtained by molecular dynamic simulation. The representation is inverted, which means dark spots corresponds to higher  $z$  levels. See text for calculation details. The lines correspond to the superstructure and the cluster direction, respectively. (b) Detail of this structure. The line joins Xe atoms on an atomic row.

perature is 30 K. The surface is cooled down to 0.5 K and is then annealed to 26 K. The equilibrium structure obtained at 26 K (Fig. 7(a)) clearly reveals a hexagonal superstructure due to the buckling of the cluster, in perfect agreement with the experimental results although inverted in height. The origin of this behavior is not clear but does not change the essential of the following discussion. The angle between the Xe cluster and the Pt(111) substrate is now 33.8°, slightly different from the initial value and the one deduced from TEAS measurements. This particular misorientation leads to an angle of about 9.5° between the superstructure pattern and the cluster structure. This is rather close to the experimental angle observed in Fig. 2(c). A detailed observation of the equilibrium structure (Fig. 7(b)) reveals that several Xe atoms (bright) are located close to on top sites and form quasi-commensurate domains. The other atoms do not sit in particular positions and form an incommensurate wall type structure. The width of this wall corresponds to about two Xe interatomic distance. A slight shift on the row direction is observed each time the row goes through an incommensurate wall leading to a small in-plane modulation of the atomic row. Unfortunately, this modulation has not been observed experimentally. A higher resolution would be required.

Molecular dynamic simulations were also performed on a small Xe island physisorbed on a Pt(111) surface. The initial condition corresponds to a cluster composed of 50 atoms aligned with respect to the Pt surface. The Xe–Xe interatomic distance is 4.55 Å and the surface temperature is 30 K. The surface is successively annealed at 39, 53, 67, 70 and 100 K and is cooled back to 34 K. We report in Fig. 8, the situation at 30, 67, 100 and 34 K. No particular structural evolution is observed up to an annealing temperature of 70 K. At 100 K, the cluster is rotated by 30° with respect to the substrate. The central part of the cluster adopts a commensurate structure whereas relaxation at the edge of the cluster is observed leading to smaller interatomic distances. The cluster keeps this structure when the surface temperature is cooled back to 34 K. This configuration seems to be an equilibrium structure since no evolution has been observed after successive annealing up to 72 K and

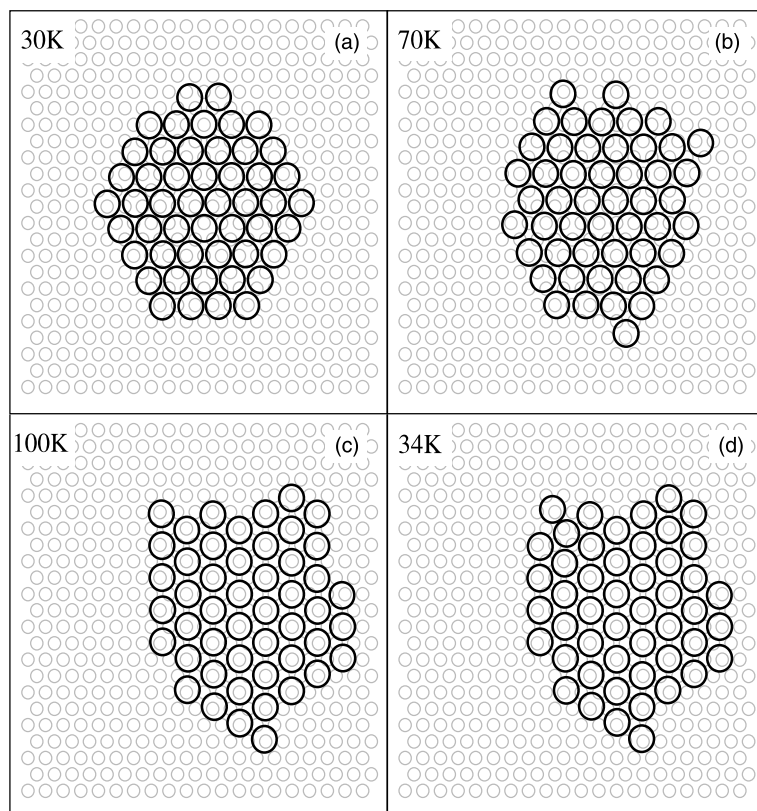


Fig. 8. Structure of an Xe island composed of 50 atoms (large circle) on a Pt(111) surface (small circle) for different annealing temperatures: (a) 30, (b) 70, (c) 100 and (d) 34 K.

cooling back to 30 K. The island orientation with respect to the Pt(111) surface is in perfect agreement with the experimental observations done on isolated Xe islands (Fig. 4). Nevertheless, the simulation does not perfectly confirm the experimental results since we have shown that the isolated islands adopt a HI structure. The resolution of the STM image (Fig. 4) does not allow us to observe a variation of the interatomic spacing within the island according to the position of the atoms. On the other hand, Weiss and Eigler [18] have recorded by STM with a high resolution a Xe island composed of 13 atoms physisorbed on a Pt(111) surface. The authors mention that the measured apparent distance between an edge atom and either a central atom or another edge atom was 10% smaller than the Xe–Xe spacing between central atoms. According to Weiss and Eigler, this

difference could be an indication of a relaxation along the island edge or a consequence of an electron redistribution toward the center of the island. The result of the simulation suggests a real variation of the interatomic spacing leading to a relaxation of the island even though one cannot a priori invalidate the electronic effect mentioned in [18].

The equilibrium interatomic distance of the Xe dimer on Pt surface predicted by molecular dynamical simulation is 4.5 Å, shorter than the observed distance. Although the influence of the tip in the experiment could be non-negligible when observing very small systems, we believe that the calculated distance is strongly questionable. The Xe/Pt(111) potential we used has been constructed on the basis of a variety of experimental data describing the interaction of single Xe atoms with a

clean surface and monolayer coverage but not from experiments where Xe atoms form very small islands on the surface. The potential probably does not present the precision and refinement necessary to describe correctly a Xe dimer on a clean Pt surface.

### 3.2. Kr on Pt(111)

Only few studies [15,37,38] concerning the structure of Kr adlayers on Pt(111) are reported. Using high-resolution He diffraction, Kern et al. [15] have uncovered the existence of a first-order phase transition between a HI ( $d_{\text{Kr-Kr}} = 4.10(2)$  Å) to an hexagonal high-order commensurate ( $d_{\text{Kr-Kr}} = 4.00(2)$  Å) layer. The phase transition occurs at a coverage  $\theta_{\text{Kr}} = 0.80$  when the surface temperature is  $T_s = 25$  K (1 ML ( $\theta_{\text{Kr}} = 1$ ) corresponds to  $7.22 \times 10^{14}$  Kr atoms/cm<sup>2</sup>). The two structural phases are both oriented by an angle of  $R30^\circ$  with respect to the substrate. Moreover, a  $(5 \times 5)R0^\circ$  superstructure has been observed on the HOC structure, due to the particular location of a fraction of the Kr atoms in fcc and hcp sites. The structure of the Kr monolayer on Pt(997) [39] is also incommensurate with a lattice parameter  $d_{\text{Kr-Kr}} = 4.00(5)$  Å but the orientations differ by  $30^\circ$ . As mentioned by the author [39], this discrepancy is probably due to the presence of a large step density on the Pt(997) surface which pins the Kr layer orientation. Indeed, the Pt(997) surface exhibits regular spaced terraces of about 20 Å width whereas the Pt(111) surface is composed of terraces of 2000–3000 Å width. The aim of the following section is to investigate the influence of the steps on the morphology of the Kr monolayer.

#### 3.2.1. Kr monolayer lying on “large” terraces

Fig. 9(a) presents an atomically resolved image of a Kr monolayer which covers a large Pt(111) terrace (at least 500 Å width). The image has been acquired after annealing the sample at 60 K. As mentioned in Section 1, the small hillocks correspond to silver clusters. The structure of the Kr adlayer is an incommensurate hexagonal structure with a lattice parameter of 4.00(2) Å in good agreement with previous results [15]. Kern et al. [15] have shown that the Kr monolayer on Pt(111)

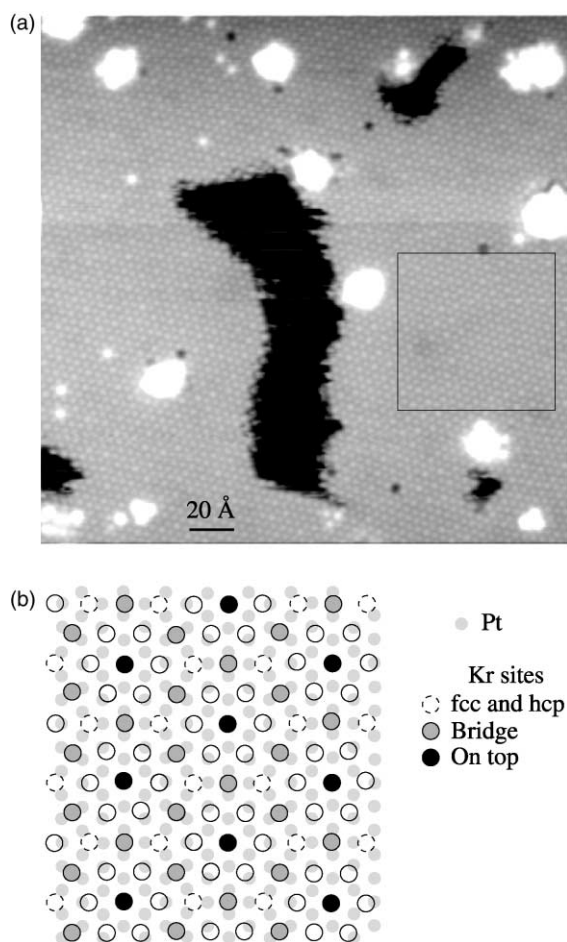


Fig. 9. (a) Kr monolayer deposited on a large Pt(111) terrace. The hillocks are silver clusters ( $V_T = -0.1$  V,  $I_T = 0.38$  nA). (b) Schematic representation of the Kr HOC structure on Pt(111).

adopts a HOC “locked” phase rotated by  $R30^\circ$  with respect to the substrate. In this phase, every sixth Kr atoms is located at a preferred adsorption site (threefold hollow) forming a hexagonal  $(5 \times 5)R0^\circ$  superstructure. The origin of such a superstructure is illustrated in Fig. 9(b), where the locked Kr layer lying on the outermost Pt layer is schematically shown. The Kr atoms in fcc (or hcp) sites (dotted circles) form a hexagonal  $(5 \times 5)R0^\circ$  superstructure. We also report in Fig. 9(b) the Kr atoms located in bridge (filled grey circles) and on top (filled black circles)-sites. Their position leads to the formation of a hexagonal  $(\frac{5}{2} \times \frac{5}{2})R0^\circ$  structure with a period  $d_s = (\frac{5}{2})d_{\text{Pt-Pt}} = \sqrt{3}d_{\text{Kr-Kr}} = 6.94$  Å.

The Kr atoms in bridge and on top-sites are located somewhat higher than the other atoms. The discrepancy in the height could be priori distinguished using a high-resolution STM. We report in Fig. 10(a) a magnification of the surface corresponding to the rectangular zone indicated in Fig. 9(a).

We notice that several Kr atoms appear brighter than the other atoms. These atoms are located at a higher position than the other ones and are distributed at specific positions on the surface. Indeed, we can clearly observe that they form a  $(\sqrt{3} \times \sqrt{3})$  hexagonal superstructure rotated by  $R30^\circ$  with respect to the Kr monolayer. For a better illustration, we report in Fig. 10(b) the

position of these specific Kr atoms: they locally form a hexagonal structure and a period  $d_{\text{super}} = \sqrt{3}d_{\text{Kr-Kr}} = 6.87(5) \text{ \AA}$  has been deduced, similar to the one obtained assuming a HOC Kr structure. This is nicely confirmed in Fig. 10(c) where two different line scans along the  $[1\ 1\ \bar{2}]$  direction of the superstructure reveal the alternation between Kr atoms sitting in on top-sites (marked by a star) and in bridge sites (marked by a circle). The on top-sites atoms are located  $0.04 \text{ \AA}$  higher than the atoms in bridge sites. This configuration is in good agreement with the schematic illustration reported in Fig. 9(b). Consequently, even though the orientation of Pt(1 1 1) is not available in this image, the observation of a  $(\sqrt{3} \times \sqrt{3})R30^\circ$  hexagonal

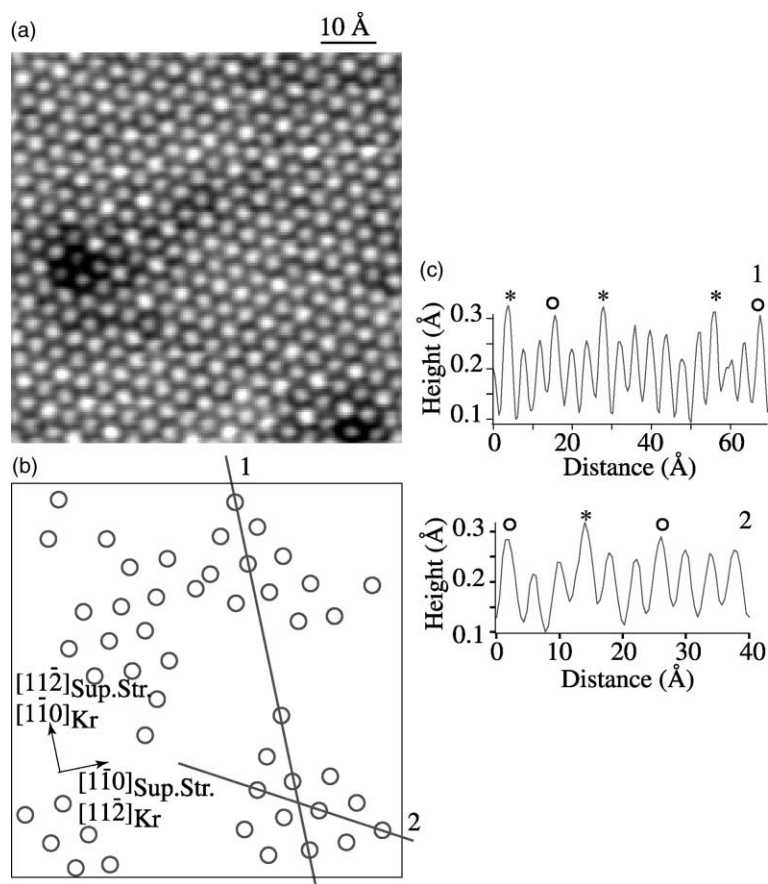


Fig. 10. (a) High magnification of the rectangular region marked in Fig. 9(a). (b) Schematic representation of the lighter atoms revealed in (a). A local hexagonal superstructure is clearly observed. (c) Line scan along two directions reported in (b). The stars and the open circles represent the on top and on bridge-sites, respectively.

superstructure corresponds well to a HOC “locked” Kr structure rotated by  $R30^\circ$  with respect to the substrate.

### 3.2.2. Influence of the steps

In order to check the influence of the steps on the Kr morphology, we have studied the structure

of the Kr monolayer adsorbed on small terraces. Fig. 11(a) shows an atomically resolved STM image of a Kr monolayer covering several Pt(111) terraces of about 50–100 Å width. The Kr monolayer structure is not a perfect hexagonal structure. Indeed we notice that the interatomic distance measured along the step edges is slightly higher

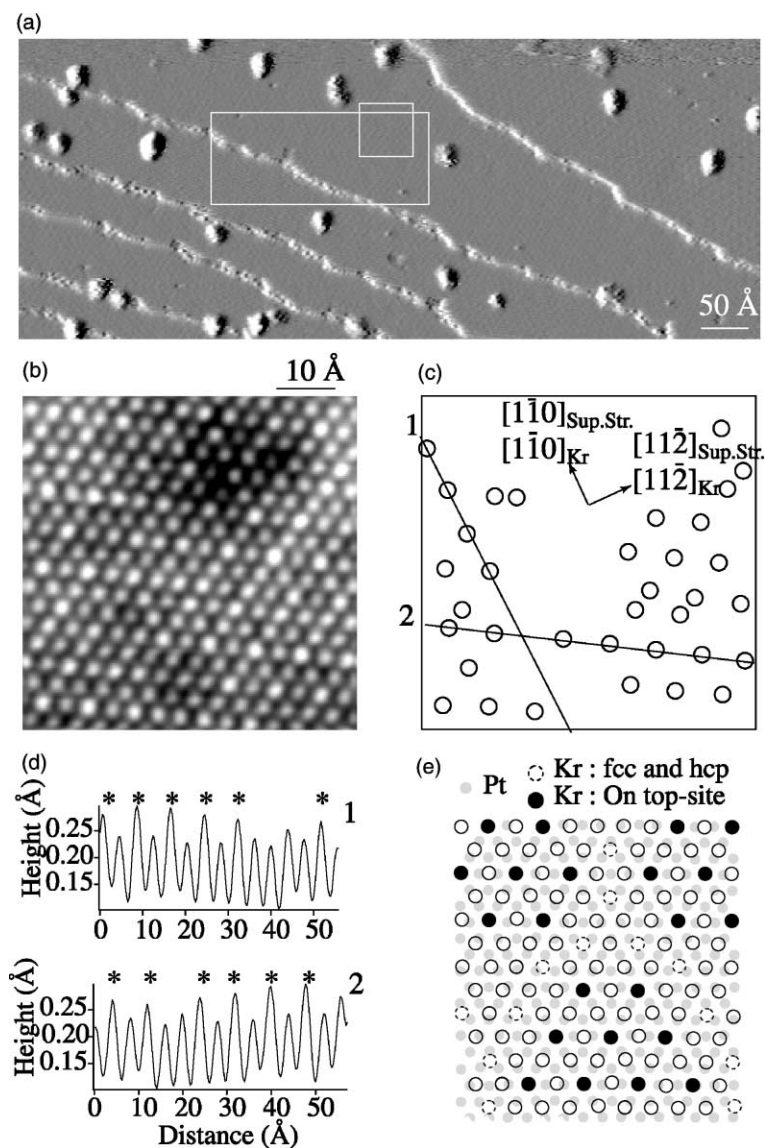


Fig. 11. (a) STM image ( $V_T = -0.17$  V,  $I_T = 0.38$  nA, derivative mode) of a Kr monolayer deposited on short terraces (50–100 Å width). (b) High magnification of the Kr monolayer ( $V_T = -0.05$  V,  $I_T = 0.75$  nA) corresponding to the square marked in (a). (c) Schematic representation of the superstructure. (d) Line scan along two directions reported in (c). (e) Model of a Kr monolayer aligned with respect to the Pt(111) surface.

than the one perpendicular to the step edges. Moreover, the discrepancy tends to be increasingly important as the terrace width is small. Fig. 11(b) is an STM image obtained in the square region reported in Fig. 11(a). The interatomic distance perpendicular to the steps is  $3.80(5)$  Å whereas it is  $4.00(5)$  Å in the two other directions. Notice that several Kr atoms are imaged higher than the others. Their position, reported in Fig. 11(c), form a hexagonal structure which is aligned with respect to the Kr monolayer. The period of this structure is  $d_s = 2d_{\text{Kr-Kr}} = 7.95(3)$  Å. We report in Fig. 11(d) two line scans obtained in two different  $[1\bar{1}0]$  directions as mentioned in Fig. 11(c). The Kr atoms which form the hexagonal structure are imaged  $0.04(1)$  Å higher than the others. An explanation is given in Fig. 11(e), where a Kr monolayer (perfect hexagonal structure with  $d_{\text{Kr-Kr}} = 4$  Å) lies on the outermost Pt(111) layer. The Kr monolayer is aligned with the Pt surface. Several Kr atoms (dotted circles) are situated in energetically favorable sites (threefold hollow) which lock the monolayer on the surface. In this model one can also notice that a superstructure is formed by Kr atoms (black circles) which are located in on-top-sites. The structure is hexagonal, aligned with the Kr monolayer, i.e. with the Pt surface, with a period  $d_{\text{super}} = 2d_{\text{Kr-Kr}} = 8$  Å ( $d_{\text{super}} \simeq 3d_{\text{Pt-Pt}}$ ) in good agreement with the observed structure in Fig. 11(b) and (c). Consequently, the structure of the Kr monolayer on this terrace is HOC but different from the  $(\frac{2}{3} \times \frac{2}{3})R0^\circ$  HOC structure observed at high coverage on large terraces. Indeed, the nearest-neighbor distance of about 4 Å (we observe a pseudo-hexagonal structure) is comparable to the HOC structure, but the orientations of the Kr monolayer differ by  $30^\circ$ .

A similar result has been obtained by Blanc [39] who have shown that the Kr monolayer on Pt(997) adopts an incommensurate hexagonal structure aligned with respect to the Pt surface. Nevertheless, our Pt surface is completely different from a Pt(997) surface which exhibits regularly spaced terraces separated by monoatomic steps, aligned with the crystallographic  $[1\bar{1}0]$  direction. In our case, the steps present in Fig. 11(a) are not aligned along a particular crystallographic direction and are composed of several kinks. We believe

that in the case of small terraces ( $\sim 50$  Å), the presence of such none well defined steps will lead to a multitude of Kr adlayer orientations. In particular it is responsible for the misorientation of the Kr adlayer adsorbed on two successive small terraces as shown in Fig. 12. This atomically resolved STM image corresponds to the rectangular zone illustrated in Fig. 11(a) and shows two Kr layers lying on two successive terraces. On the lower terrace, the Kr adlayer adopts a pseudo-hexagonal structure with an interatomic distance of  $3.90(5)$  and  $4.20(5)$  Å perpendicular and along the step, respectively. One observes that the Kr adlayers adsorbed on the lower and the upper terrace are not aligned and are rotated by an angle of  $11^\circ$ . A qualitative explanation of this rotation is schematically shown in Fig. 12(b). The step is composed of several (111)-microfacet steps (three Pt atoms width) separated by monoatomic kinks, leading to an angle of about  $19^\circ$  between the mean direction of the step and the  $[1\bar{1}0]$  direction.

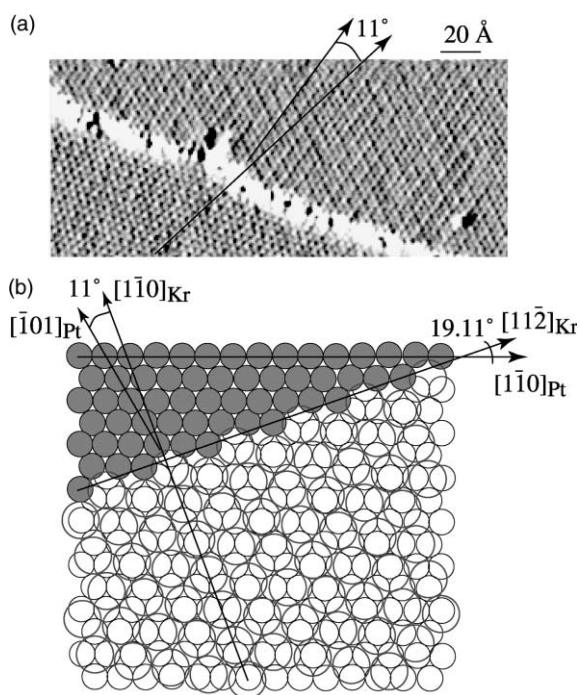


Fig. 12. (a) STM image ( $V_T = -0.170$  V,  $I_T = 0.38$  nA, derivative mode) corresponding to the rectangular part marked in Fig. 10(a). (b) Schematic model revealing the influence of the step edge on the Kr adlayer orientation.

During the first stage of the growth, an incoming Kr atom will tend to maximize its coordination with Pt atoms at the step edge. Consequently, it is reasonable to assume that the kinks will pin the first incoming Kr atoms. The other Kr atoms will tend to establish a natural interatomic distance ( $\approx 4 \text{ \AA}$ ) with the first adsorbed Kr atoms. This leads to the formation of a pseudo-hexagonal structure where the  $[11\bar{2}]_{\text{Kr}}$  direction is aligned with the mean direction of the step as mentioned in Fig. 12(b). As a consequence, the Kr adlayer is rotated by about  $11^\circ$  with respect to substrate orientation. This configuration is stable from an energetical point of view since several Kr atoms are located on hollow sites. Moreover, a heat of adsorption of 210(10) meV of the first Kr monolayer on Pt(997) has been obtained [39], which is substantially higher than the one obtained on Pt(111) (158(4) meV [40]). The excess of binding energy can be attributed to an increased adsorbate–substrate interaction. The attraction of the step can play an important role even though calculations [39] done for Xe on Pt(997) have shown that the excess attraction of the step fades away after two rows. Nevertheless, the role of the step and more precisely the nature of the step (well defined or irregular shape with kinks) appears to be critical for the structure of the Kr adlayer. The STM image (Fig. 12(a)) and its simple model (Fig. 12(b)) show that the morphology of the step can lead to the growth of misoriented Kr adlayer with respect to the substrate.

### 3.2.3. Kr submonolayer and step edges decoration

Raising the surface temperature to 125 K results in evaporation of the Kr atoms from the terraces. Fig. 13(a) and (b) show this situation where only higher coordinated Kr atoms on step edges and adsorbates (silver clusters) are observed. We can also observe few isolated Kr atoms lying on the surface. We find a multiple row structure at the step edge and a monorow structure around most of the adsorbates. The decoration of adsorbates by Kr atoms will be discussed in detail in forthcoming publications [27,29]. The terraces are about  $50 \text{ \AA}$  width and the step edges are relatively regular, a morphology which is similar to the one observed on a (997) Pt surface. The presence of

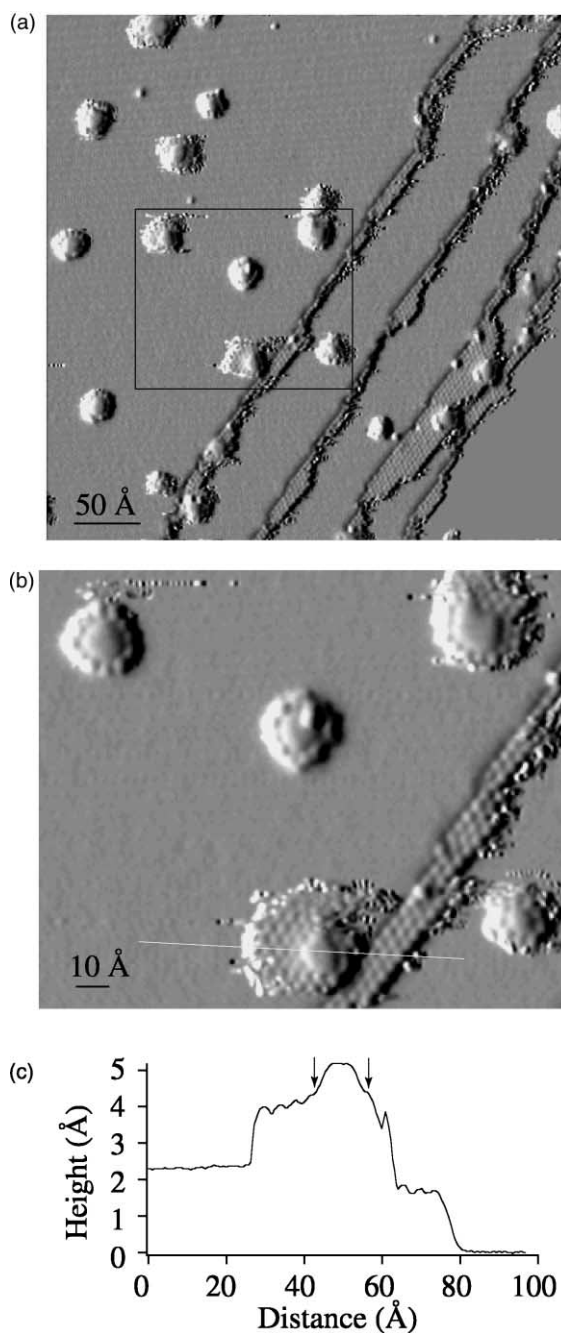


Fig. 13. (a) STM image ( $V_T = -0.200 \text{ V}$ ,  $I_T = 0.38 \text{ nA}$ , derivative mode) recorded after annealing the sample at 125 K with several silver clusters and step edges decorated by Kr atoms. (b) shows a magnification (rectangular zone in (a)) over several silver clusters and a step edge decorated by three Kr rows. (c) Line profile from left to right as indicated in (b).

few kinks do not affect the Kr structure since we find that the rows are perfectly aligned with respect to the  $[1\bar{1}0]_{\text{Pt}}$  direction. The Kr atoms form a  $\text{HI } R0^\circ$  structure with an interatomic distance of  $4 \text{ \AA}$  in perfect agreement with a previous study [39]. This result confirms the crucial role of the step edges on the Kr structure, specifically on its orientation with respect to the substrate, as already mentioned in Section 3.2. Krypton atoms decorating the steps are imaged  $1.70(5) \text{ \AA}$  high (Fig. 13(c)) compared to  $0.9(2) \text{ \AA}$  for isolated Kr atoms. It should again be stressed that the apparent height of the rare gases measured by STM does not reflect the “physical” or the crystallographic height but correspond to an “electronic” height. Electronic effects can affect the apparent height, in particular if different species are present. That is the reason why the apparent Kr height changes according to its position from the silver cluster (Fig. 13(c)). The nearest Kr atoms (marked by an arrow) are imaged  $1.9(1) \text{ \AA}$  whereas the Kr atoms at the periphery are imaged  $1.70(5) \text{ \AA}$ , i.e. the same height measured for Kr atoms decorating the steps.

### 3.3. Ar on Pt(111)

To our knowledge, the structure of Ar physisorbed on Pt(111) in the submonolayer coverage regime has only been explored by thermal He-atom scattering [12]. At coverage  $\theta_{\text{Ar}} \leq 0.7 \text{ ML}$  the Ar condenses in a hexagonal close-packed phase with domains aligned with the substrate with a lattice parameter of about  $3.81 \text{ \AA}$ . With increasing the coverage ( $\theta_{\text{Ar}} \geq 0.7 \text{ ML}$ ), a first-order phase transition into a compressed hexagonal Ar phase with a lattice parameter of  $3.70 \text{ \AA}$  is observed. The compressed phase is a HOC phase, characterized by a  $(4 \times 4)R0^\circ$  commensurate unit cell. This series of HOC phases has been explained by potential calculations of Ramseyer et al. [41].

#### 3.3.1. Ar monolayer

The STM topograph in Fig. 14(a) shows an atomically resolved Ar monolayer ( $\theta_{\text{Ar}} = 1$  correspond to  $7.87 \times 10^{14} \text{ Ar atoms/cm}^2$ ). The Ar atoms adopt a hexagonal structure with a nearest-neighbor distance of  $3.83(6) \text{ \AA}$ . A magnification of the

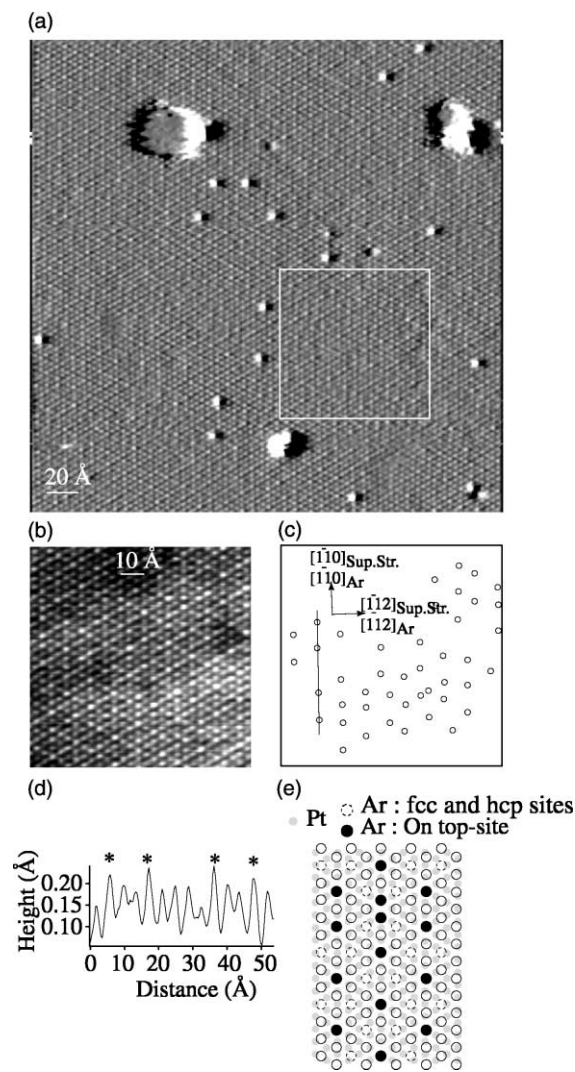


Fig. 14. (a) STM image ( $V_T = -0.181 \text{ V}$ ,  $I_T = 0.38 \text{ nA}$ , derivative mode) of a Ar monolayer. (b) High magnification of the monolayer corresponding to the square region in (a). (c) Schematic representation of the observed superstructure. (d) Line scan along the direction marked in (c). (e) Model of a HOC Ar layer on a Pt(111) surface.

surface (Fig. 14(b)) reveals a  $(4 \times 4)$  hexagonal superstructure aligned with the Ar monolayer with a periodicity of  $4a_{\text{Pt}} = 3a_{\text{Ar}}$ . As mentioned in (Fig. 14(c) and (d)), the Ar atoms which are located at a higher position than the other ones ( $0.04(1) \text{ \AA}$  higher), locally form a hexagonal structure with a period of  $d_{\text{super}} = 3d_{\text{Ar-Ar}} = 11.50(5) \text{ \AA}$ . The

observation of such a superstructure is in good agreement with the  $(4 \times 4)R0^\circ$  superstructure deduced from TEAS measurements [12] corresponding to a HOC structure. This situation is shown in Fig. 14(e), where the locked Ar layer ( $d_{\text{Ar-Ar}} = 3.8 \text{ \AA}$ ) lying on the outermost Pt layer is schematically represented. We clearly observe that the Ar atoms in on top-sites form locally a hexagonal structure with a period  $d_{\text{super}} = 3d_{\text{Ar-Ar}}$ . The superstructure is aligned with the Ar layer, in perfect agreement with our STM observations.

### 3.3.2. Ar submonolayer

A submonolayer regime has been observed after annealing the surface at 50 K. The situation is shown in Fig. 15(a) and (b), where several isolated close-packed Ar islands with a mean size of about  $6500 \text{ \AA}^2$  are adsorbed on terraces and step edges. Whatever the island, the measured  $d_{\text{Ar-Ar}}$  interatomic distance is  $3.90(5) \text{ \AA}$ , slightly higher than the one observed for the monolayer, in good agreement with TEAS measurements [12]. The height of the islands is  $1.15(5) \text{ \AA}$  which is similar

to height of the monolayer measured in Fig. 14(a). The most interesting feature revealed in these images is that the islands adopt several orientations with respect to the Pt(1 1 1) surface. The measured orientations, reported in Fig. 15(a) and (b), are  $R0^\circ$ ,  $R7.5^\circ$ ,  $R15^\circ$ ,  $R30^\circ$ ,  $R31.9^\circ$ ,  $R33.8^\circ$ ,  $R45^\circ$  and  $R52.5^\circ$  which are found to be all a multiple of  $1.875^\circ$ . This result suggest that, for low coverage, the most energetically favorable position for the Ar atoms correspond to a  $R(1.875 \times n)^\circ$  ( $n$  an integer number) hexagonal structure with a lattice parameter of about  $3.9 \text{ \AA}$ . From our measurements we cannot confirm if these structures are locked or not. For such low coverage, the observations reported by Zeppenfeld et al. [12] are slightly different. For  $\theta_{\text{Ar}} = 0.36 \text{ ML}$ , depending of the annealing temperature and annealing time, several Ar HOC structures with different lattice parameter (in the range between  $3.6$  and  $3.9 \text{ \AA}$ ) have been observed. Nevertheless, whatever the observed hexagonal HOC structures, it has been shown that the Ar phases are aligned with respect to the Pt(1 1 1) surface.

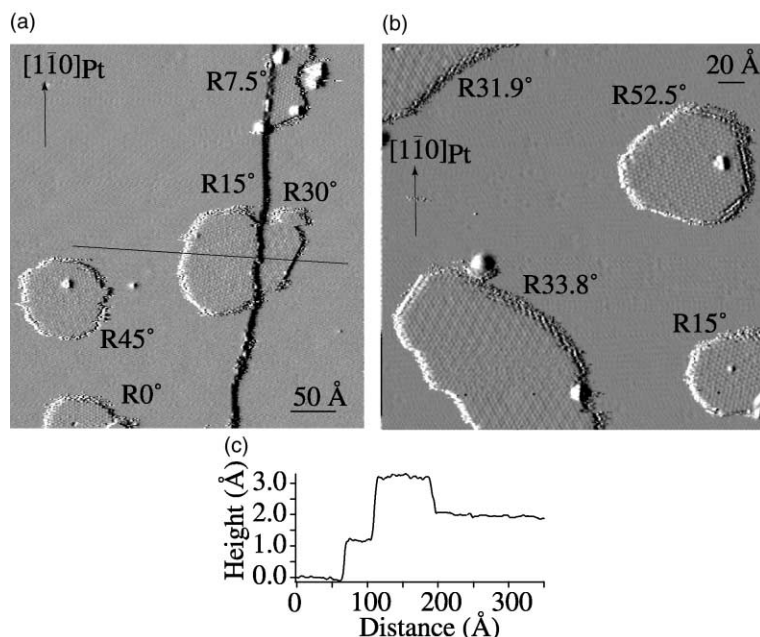


Fig. 15. (a, b) STM images ( $V_T = -0.724 \text{ V}$ ,  $I_T = 0.12 \text{ nA}$  and  $V_T = -0.965 \text{ V}$ ,  $I_T = 0.38 \text{ nA}$ , respectively, derivative mode) of Ar islands. (c) Line scan from right to left, along the direction marked in (a).

#### 4. Conclusion

We have studied submonolayer coverages of Xe, Kr and Ar physisorbed on a Pt(111) surface using low-temperature STM. The possibility of direct imaging of the rare gas atoms has enabled us to follow the phase transition occurring with coverage changes.

The Xe adlayer structure is strongly dependent on the coverage of the surface and the sequence HIR  $\rightarrow$  HI transition with decreasing the rare gas coverage has been observed unambiguously. A critical Xe island size defining the onset of the adlayer rotation has been deduced. Xe monomers and dimers have also been imaged on the surface. No energetic favorable positions of the monomer and the dimer have been observed. Nevertheless, it has been shown that the dimers adopt a commensurate structure on the surface with a Xe atom separation which is twice the Pt interatomic distance in disagreement with ab initio calculations.

The step morphology influences the orientation of the Kr monolayer with respect to the substrate. In a surface area composed of narrow terraces, different orientations of the Kr HI structure have been observed and depend on the nature of the step (well defined or irregular shape with kinks). A different situation is observed on large terraces since the Kr monolayer adopts a HOC  $R30^\circ$  structure.

In the submonolayer-coverage regime, the Ar islands condense in a HI close-packed phase domain. At monolayer completion, the HI structure transforms to a compressed HOC structure aligned with respect to the substrate.

The structural features reported in this paper constitute an interesting support for theoretical studies performed on rare gases (Xe, Kr and Ar) physisorbed on Pt(111) since direct comparison between calculations and real-space observations are possible.

#### Acknowledgements

This work was supported by the Swiss National Fund.

#### References

- [1] M. Bienfait, J.L. Seguin, J. Suzanne, E. Lerner, J. Krim, J.G. Dash, Phys. Rev. B 29 (1984) 983.
- [2] K. Kern, G. Comsa, in: R. Vanselow, R.F. Howe (Eds.), Chemistry and Physics of Solid Surface VII, Springer Series in Surface Science, Springer-Verlag, New York, 1988.
- [3] B. Poelsma, L. Verheij, G. Comsa, Surf. Sci. 152–153 (1985) 851.
- [4] K. Kern, R. David, P. Zeppenfeld, G. Comsa, Surf. Sci. 195 (1988) 353.
- [5] K. Kern, R. David, L. Palmer, G. Comsa, Surf. Sci. 175 (1986) L669.
- [6] K. Kern, P. Zeppenfeld, R. David, G. Comsa, J. Vac. Sci. Technol. A 6 (1988) 639.
- [7] B. Grimm, H. Hövel, M. Pollman, B. Reihl, Phys. Rev. B 83 (1999) 991.
- [8] E. Specht et al., Z. Phys. B 69 (1987) 347.
- [9] H. Hong, C. Peters, A. Mak, R. Birgeneau, P. Horn, H. Suematsu, Phys. Rev. B 40 (1989) 4797.
- [10] M. Hamichi, A. Faisal, J. Venables, R. Kariotis, Phys. Rev. B 39 (1989) 415.
- [11] G. Bracco, P. Cantini, A. Glachant, R. Tatarek, Surf. Sci. 125 (1983) L81.
- [12] P. Zeppenfeld, U. Becher, K. Kern, G. Comsa, Phys. Rev. B 45 (1992) 5179.
- [13] K. Kern, R. David, R.L. Palmer, G. Comsa, Phys. Rev. Lett. 56 (1986) 2823.
- [14] K. Kern, Phys. Rev. B 35 (1987) 8265.
- [15] K. Kern, P. Zeppenfeld, R. David, G. Comsa, Phys. Rev. Lett. 59 (1987) 79.
- [16] K. Kern, R. David, R. Palmer, G. Comsa, Phys. Rev. Lett. 56 (1986) 620.
- [17] K. Kern, R. David, R. Palmer, G. Comsa, Appl. Phys. Lett. 59 (1987) 79.
- [18] P.S. Weiss, D.M. Eigler, Phys. Rev. Lett. 69 (1992) 2240.
- [19] P. Zeppenfeld, S. Horch, G. Comsa, Phys. Rev. Lett. 73 (1994) 1259.
- [20] D.M. Eigler, P.S. Weiss, E.K. Schweizer, N.D. Lang, Phys. Rev. Lett. 66 (1991) 1189.
- [21] S. Horch, P. Zeppenfeld, R. David, G. Comsa, Rev. Sci. Instrum. 65 (1994) 3204.
- [22] S. Horch, P. Zeppenfeld, G. Comsa, Appl. Phys. A 60 (1995) 147.
- [23] S. Horch, P. Zeppenfeld, G. Comsa, Surf. Sci. 331–333 (1995) 908.
- [24] M. Dienwiebel et al., Surf. Sci. 446 (2000) L113.
- [25] J.Y. Park et al., Phys. Rev. B 60 (1999) 16934.
- [26] H. Jödicke, R. Schaub, R. Monot, J. Buttet, W. Harbich, Rev. Sci. Instrum. 71 (2000) 2818.
- [27] R. Schaub, H. Jödicke, F. Brunet, R. Monot, J. Buttet, W. Harbich, to be published.
- [28] K. Kern, R. David, R. Palmer, G. Comsa, Phys. Rev. B 56 (1986) 2823.
- [29] R. Schaub, F. Brunet, R. Monot, J. Buttet, W. Harbich, Phys. Rev. Lett. 86 (2001) 3590.

- [30] A. Novaco, J. McTague, *Phys. Rev. Lett.* 38 (1977) 1286.
- [31] R.J. Muirhead, J.G. Dash, J. Krim, *Phys. Rev. B* 29 (1984) 5074;  
J. Krim, J.G. Dash, J. Suzanne, *Phys. Rev. Lett.* 52 (1984) 640;  
D.A. Huse, *Phys. Rev. B* 29 (1984) 6985.
- [32] J. Barker, R. Watts, J. Lee, T. Schafer, Y. Lee, *J. Chem. Phys.* 61 (1974) 3081.
- [33] J.E. Müller, *Phys. Rev. Lett.* 65 (1990) 3021.
- [34] J. Barker, C. Rettner, *J. Chem. Phys.* 97 (1992) 5844.
- [35] J. Barker, C. Rettner, *J. Chem. Phys.* 101 (1994) 9202.
- [36] B.L. Maschhoff, J.P. Cowin, *J. Chem. Phys.* 101 (1994) 8138–8151.
- [37] H. Hannemann, Forschungszentrum Jülich, Germany, 1997.
- [38] L. Bruch, A. Graham, J. Toennies, *J. Chem. Phys.* 112 (2000) 3314.
- [39] M. Blanc, Ph.D. Thesis, EPFL, 1998.
- [40] P. Zeppenfeld, Diploma Thesis, Universität Bonn, 1989..
- [41] C. Ramseyer, P. Hoang, C. Girardet, *Phys. Rev. B* 49 (1994) 2861.